Shear-Induced Reorganization of Deformable Molecular Assemblages: Monte Carlo Studies

Albert S. Kim,[†] Subir Bhattacharjee,*[,‡] and Menachem Elimelech[‡]

Department of Chemical Engineering, P.O. Box 208286, Yale University, New Haven, Connecticut 06520-8286 and School of Engineering and Applied Science, University of California, Los Angeles, California 90095-1593

Received August 2, 2000. In Final Form: October 26, 2000

The influence of hydrodynamic shear on the shape of deformable molecular assemblages is studied using Monte Carlo simulations. Metropolis Monte Carlo simulations are performed to generate spherical assemblages of amphiphilic molecules by considering coarse statistical mechanical models for the various constituent subunits of the amphiphiles and by avoiding explicit consideration of the solvent molecules. The resulting assemblage is subjected to a unidirectional hydrodynamic shear, and the transition of the system to a secondary equilibrium is studied using a modified Monte Carlo simulation technique that accounts for the systematic force on the assemblage due to the hydrodynamic shear. The influence of hydrodynamic shear on the shape of the assemblage is described qualitatively through several simulation snapshots. The quantitative analysis suggests that the aggregate size, intermolecular interactions between various subunits, and shear rate govern the extent of shear-induced deformation. The three parameters can be combined using a single dimensionless group, the Peclet number. Results indicate that the Peclet number can provide considerable insight into the nature and extent of structural deformation of molecular assemblages in the presence of hydrodynamic shear. There exists a critical Peclet number below which hydrodynamic shear has no effect on the aggregate structure. Above the critical Peclet number, the aspect ratio (a measure of deformation) of the assemblage increases almost linearly with logarithm of the Peclet number.

1. Introduction

Molecular assemblages such as micelles, vesicles, microemulsion, and emulsion droplets are essentially "soft" or deformable entities. Such molecular assemblages are generally formed by amphiphilic molecules such as surfactants and polyelectrolytes, and are often employed for encapsulation or solubilization of various organic or ionic species in aqueous systems.[1] Application of molecular assemblages is gaining prominence in environmental,[2−6] pharmaceutical,[7−9] and biological[10] processes. The equilibrium thermodynamics of molecular assembly depends on the molecular interactions among the amphiphiles and the solvent. The equilibrium structure of such assemblages generally evolves from the propensity of the lyophobic and lyophilic regions of the amphiphiles to partition into a solvent-depleted and a solvent-rich phase, respectively.[11,12] For instance, polar (or hydrogen bonding) interactions between the polar headgroups of the amphiphiles and the solvent molecules coupled with the hydrophobic attraction between the tail groups of the amphiphile leads to the formation of micelles in aqueous media.[12] The typical entropic and energetic contributions leading to the formation of various shapes of the amphiphilic clusters may be appraised using classical thermodynamic principles to some extent.[11,12] However, in many dynamic processes, for instance, during cross-flow membrane filtration,[13,14] in stirred tank reactors, or pipelines, such deformable entities are subject to hydrodynamic shear fields of varying magnitudes,[15,16] making it difficult to apply classical thermodynamic approaches to study the shear-induced deformation of such assemblages.

Several approaches of studying the clustering of amphiphilic molecules and encapsulation of organic or ionic species in the resulting assemblages are available. These approaches can be broadly categorized into those based on classical thermodynamics,[11,12] statistical mechanical theories using lattice approaches,[17−20] and computer

* Corresponding author (tel.: (203) 432 4333; fax: (203) 432 2895; E-mail: subir.bhattacharjee@yale.edu).

[†] University of California.

[‡] Yale University.

(1) Elworthy, P. H.; Florence, A. T.; Macfarlane, C. B. *Solubilization by Surface-Active Agents*; Chapman and Hall: London, 1968.

(2) Scamehorn, J. F.; Harwell, J. H. In *Surfactants in Chemical/Process Engineering*; Wasan, D. T., Ginn, M. E., Shah, D. O., Eds.; Marcel Dekker: New York, 1988; p 77.

(3) Christian, S. D.; Scamehorn, J. F. In *Surfactant Based Separation Processes*; Scamehorn, J. F., Harwell, J. H., Eds.; Marcel Dekker: New York, 1989, p 3.

(4) Markels, J. H.; Radke, C. J. *J. Membrane Sci.* **1994**, *86*, 241.

(5) Dunn, R. O., Jr.; Scamehorn, J. F.; Christian, S. D. *Sep. Sci. Technol.* **1985**, *20*, 257.

(6) Dunn, R. O., Jr.; Scamehorn, J. F.; Christian, S. D. *Colloids Surf.* **1989**, *35*, 49.

(7) Speiser, P. In *Reverse Micelles: Biological and Technological Relevance of Amphiphilic Structures in Apolar Media*; Luisi, P. L., Straub, B. E., Eds.; Plenum Press: New York, 1984; p 339.

(8) Lawrence, M. J. *Chem. Soc. Rev.* **1994**, *23*, 417.

(9) Attwood, D. In *Colloidal Drug Delivery Systems*; Kreuter, J., Ed.; Marcel Dekker: New York, 1994; p 31.

(10) Hatton, T. A. In *Surfactant Based Separation Processes*; Scamehorn, J. F., Harwell, J. H., Eds.; Marcel Dekker: New York, 1989; p 57.

(11) Nagarajan, R.; Chaiko, M. A.; Ruckenstein, E. *J. Phys. Chem.* **1984**, *88*, 2916.

(12) Israelachvili, J. N. *Intermolecular and Surface Forces*; Academic Press: New York, 1991.

(13) Markels, J. H.; Lynn, S.; Radke, C. J. *AIChE J.* **1995**, *41*, 2058.

(14) Scamehorn, J. F.; Christian, S. D.; Tucker, E. E.; Bernadette, I. T. *Colloids Surf.* **1990**, *49*, 259.

(15) van de Ven, T. G. M. *Colloidal Hydrodynamics*; Academic Press: San Diego, 1989.

(16) Smith, P. G.; van de Ven, T. G. M. *Colloids Surf.* **1985**, *15*, 191.

(17) Flory, P. J. *Principles of Polymer Chemistry*; Cornell University Press: Ithaca, 1953.

(18) Marqusee, J. A.; Dill, K. *J. Chem. Phys.* **1986**, *85*, 434.

(19) Hurter, P. N.; Scheutjens, J. M. H. M.; Hatton, T. A. *Macromolecules* **1993**, *26*, 5592.

(20) Gelbart, W. M.; Roux, D.; Ben-Shaul, A., Eds. *Micelles, Membranes, Microemulsions, and Monolayers*; Springer-Verlag: Berlin, 1995.

10.1021/la001108v CCC: $20.00
Published on Web 12/23/2000

simulations.[21−30] The computer simulation approach is particularly advantageous, because it does not require a priori assumptions regarding the shapes and structures of the clusters. In addition, computer simulations allow greater flexibility regarding the molecular level details that can be incorporated into the models.

Computer simulations can be performed at various levels of complexity, depending on the sophistication of the molecular model of the system under consideration. The molecular model is primarily concerned with the specification of the interaction potentials between the different molecular species comprising a system. Although such simulations can be performed at the scale of the "exact" molecular architecture of every species including the solvent,[26,27] the enormous requirement of computational resources has precluded their widespread application to date. On the other hand, such simulations can also be performed at the coarsest possible level by considering the particle nature of only the largest species, and by indirectly incorporating the effects of the solvent and other smaller species through appropriate continuum level potentials of mean force between the largest species.[28−32] Note that such coarse potentials can substantially simplify the simulations by considering fewer types of molecular species.

Simulations involving amphiphilic molecules, particularly those aiming toward studying the formation of clusters in such systems, are generally based on models that lie between these two extremes. Such simulations are generally performed by defining various subunits in the amphiphilic molecule as individual species and often by explicitly considering the solvent molecules. Although coarser than the exact models, these models also pose a considerable computational burden arising from the requirement of including a large number of solvent molecules in the simulation. Computer simulations using such intermediate models may be lattice based[21−25] or may not consider a lattice ("off-latice simulations").[33,34] Lattice-based Monte Carlo (MC) simulations have been widely applied for studying micellization of surfactants, copolymer solutions, phase equilibria in surfactant-oil−water systems, and micellar encapsulation.[21−25] "Off-lattice" computer simulations have been used less frequently to study the equilibrium behavior of molecular assemblages.[33,34] In this light, it is discernible that little progress has been made in understanding the deformation of such assemblages under the influence of external forces, particularly hydrodynamic shear.

Although computer simulation of rigid particles in an external force field (for instance, in the presence of hydrodynamic shear) is quite common,[30] it is considerably difficult to simulate the structural modifications of a deformable assemblage in the presence of such external forces. Any computer simulation inherently assumes the particles to be rigid, with the interaction potential depending on the shape, position, and orientation of the particle. Both the particle shape and the interaction potential cannot be simultaneously adjusted during a computer simulation. Thus, for a deformable assemblage, such simulations must consider the assemblage to be made up of rigid subunits. The influence of any externally imposed shear on the shape of the aggregate may then be simulated by considering the dynamics of the individual subunits under the shear field.

There have been a few recent off-lattice simulations on deformation of molecular assemblages in the presence of hydrodynamic shear using MC methods.[35,36] Such techniques have generally employed a systematic bias in the direction of the shear, although such a bias has not been based on the intensity of the flow.[35] It should be noted that when an assemblage is subjected to unidirectional shear, the movement of regions of the assemblage closer to the center will be influenced to a lesser extent by the shear compared to regions that exist near the periphery of the assemblage. The objective of the present study is to incorporate such a spatially varying influence of shear on the biased moves of the particles.

In this study, we develop a methodology for performing Monte Carlo simulations of the shear-induced deformation of a molecular aggregate. Toward this, the first task is to design a model of the molecular assemblage that yields a realistic equilibrium configuration of the assemblage in the absence of external shear forces. The equilibrium configuration is obtained using a coarse model of the various molecular groups forming an amphiphilic chain, without explicitly considering the solvent molecules. This approach, apart from simplifying the simulation procedure, facilitates the incorporation of hydrodynamic shear as a uniform external force acting on the molecular groups (subunits) constituting the assemblage. Monte Carlo simulations are then performed on these assemblages to study their deformation under the influence of hydrodynamic shear. These simulations are performed using a modified Metropolis technique that incorporates the hydrodynamic shear as a systematic external force acting on the individual subunits to bias their moves.

2. Model of a Molecular Assemblage

A typical deformable assemblage is composed of several surfactant or polyelectrolyte chains, each having a polar (generally charged) headgroup and a long nonpolar tail predominantly comprising several repetitive units in an alkyl chain.[12] Such amphiphilic chains, when suspended in the solvent, organize into a lyophobic core containing the tail subunits and a lyophilic surface containing the headgroups.[12] The molecular architecture of a complex chain and the solvent molecules is too cumbersome to incorporate in a computer simulation of an aggregate. Consequently, several simplified models for the interaction potentials between various subunits of the amphiphilic chain have been formulated.[22,25,37] In lattice-based simulations, only nearest neighbor interactions are considered, leading to the identification of three independent bond parameters, namely, the head−head, head−solvent, and tail−solvent interactions.[22,37] Furthermore, in such simulations, the nearest neighbor bonds are considered to have

(21) Larson, R. G. *J. Chem. Phys.* **1992**, *96*, 7904.
(22) Desplat, J. C.; Care, C. M. *Mol. Phys.* **1996**, *87*, 441.
(23) Wang, Y.; Mattice, W. L.; Napper, D. H. *Langmuir* **1993**, *9*, 66.
(24) Wijmans, C. M.; Linse, P. *Langmuir* **1995**, *11*, 3748.
(25) Talsania, S. K.; Wang. Y.; Rajagopalan, R.; Mohanty, K. K. *J. Colloid Interface Sci.* **1997**, *190*, 92.
(26) Karaborni, S.; van Os, N. M.; Esselink, K.; Hilbers, P. A. J. *Langmuir* **1993**, *9*, 1175.
(27) Karaborni, S.; Esselink, K.; Hilbers, P. A. J.; Smit, B. *J. Phys.: Condens. Matter* **1994**, *6*, 351.
(28) Metropolis, N.; Rosenbluth, A. W.; Rosenbluth, M. N.; Teller, A. H.; Teller, E. *J. Chem. Phys.* **1953**, *21*, 1087.
(29) Ermak, D. L.; McCammon, J. A. *J. Chem. Phys.* **1978**, *69*, 1352.
(30) Brady, J. F.; Bossis, G. *Annu. Rev. Fluid Mech.* **1988**, *20*, 111.
(31) Allen, M. P.; Tildesley, D. J. *Computer Simulation of Liquids*; Clarendon Press: Oxford, U.K., 1987.
(32) Rao, K. S.; Salgi, P.; Rajagopalan, R. *Ind. Eng. Chem. Res.* **1996**, *35*, 2909.
(33) Smit, B.; Hilbers, P. A. J.; Esselink, K.; Rupert, L. A. M.; van Os, N. M. *J. Phys. Chem.* **1991**, *95*, 6361.
(34) Rector, D. R.; van Swol, F.; Henderson, J. R. *Mol. Phys.* **1994**, *82*, 1009.
(35) Lai, P. Y.; Binder K. *J. Chem. Phys.* **1993**, *98*, 2366.
(36) Milcher, A.; Binder, K. *Langmuir* **1999**, *15*, 3232.
(37) Care, C. M. *J. Phys. Chem.* **1987**, *20*, 689.

a constant energy.[25] In nonlattice simulations, the interactions are usually modeled using truncated Lennard−Jones type interaction potentials.[33,34] In this study, we employ a simplified version of the latter approach to formulate the interaction potential between various subunits of an amphiphilic chain without explicitly considering the solvent molecules. Furthermore, the molecular architecture of the amphiplilic chains is considerably simplified by assuming these chains to be composed of a single spherical headgroup and a cluster of spherical tail groups.

The amphiphilic chain is considered to have n subunits with one subunit being a charged headgroup and the remaining $n - 1$ subunits being the tail groups. The interaction potentials between the various subunits were modeled on the basis of Lennard−Jones potential (representing the dispersion interactions), Coulomb potential for the electrostatic interactions between the ionic headgroups, and two additional interactions which will be described in detail below. These additional potentials emulate the hydrogen bonding interactions between the assemblage and the polar solvent molecules. Thus, in the present study, explicit consideration of the solvent molecules is avoided, although the interactions leading to the formation of the amphiphilic cluster are considered in terms of "pseudo-potentials".

Neglecting any specific bond interactions, that is, without distinguishing between interchain and intrachain interactions,[22] the tail−tail (TT) and the tail−head (TH) interaction energies are represented using a Lennard−Jones type interaction potential as[31]

$$U_{TT} = 4\epsilon_{TT}\left[\left(\frac{\sigma_{TT}}{r}\right)^{12} - \left(\frac{\sigma_{TT}}{r}\right)^{6}\right] \quad (1)$$

and

$$U_{TH} = 4\epsilon_{TH}\left[\left(\frac{\sigma_{TH}}{r}\right)^{12} - \left(\frac{\sigma_{TH}}{r}\right)^{6}\right] \quad (2)$$

where r is the center to center distance between the two groups, ϵ_{TT} and ϵ_{TH} are the Lennard−Jones parameters for the interaction between two tail groups, and between the tail and headgroups, respectively, σ_{TT} is the diameter of the tail group, and $\sigma_{TH} = 0.5(\sigma_T + \sigma_H)$ is the center-to-center distance between the tail and headgroups at contact.

The interaction between two headgroups (U_{HH}) can be obtained by combining the repulsive Lennard−Jones and Coulomb potentials[31]

$$U_{HH} = 4\epsilon_{HH}\left(\frac{\sigma_{HH}}{r}\right)^{12} + \frac{z^2e^2}{4\pi\epsilon_0\epsilon_r}\frac{1}{r} \quad (3)$$

where ϵ_{HH} is the Lennard−Jones parameter for the interaction between two headgroups, σ_{HH} is the diameter of the headgroup, z is the charge number of the headgroup, e is the electronic charge, ϵ_0 is the dielectric permittivity of vacuum, and ϵ_r is the relative dielectric permeability of the solvent medium.

In addition, two kinds of external interactions were employed to emulate the solvent effects that lead to the formation of the amphiphilic assemblage. First, the "spherical boundary condition"[38,39] was used to prevent the subunits from escaping the simulation cell. A Lennard−Jones type interaction given by

$$\begin{aligned} U_{ex} &= 4\epsilon_{ex}\left[\left(\frac{\sigma_{ex}}{r_{wall} - r}\right)^{12} - \left(\frac{\sigma_{ex}}{r_{wall} - r}\right)^{6}\right] - U^0_{ex} \quad \text{for } r_{ran} < r < r_{wall} \\ U_{ex} &= 0 \quad \text{otherwise} \end{aligned} \quad (4)$$

where

$$U^0_{ex} = 4\epsilon_{ex}\left[\left(\frac{\sigma_{ex}}{r_{wall} - r_{ran}}\right)^{12} - \left(\frac{\sigma_{ex}}{r_{wall} - r_{ran}}\right)^{6}\right] \quad (5)$$

was used to model the interaction of the subunits with the spherical boundary. In the above equation, r_{wall} is the radius of the spherical simulation cell, which is the sum of r_{ran} and σ_{ex}. The parameter r_{ran} is calculated by

$$r_{ran} = \left(\frac{\sigma_{TT}}{2}\right)\left(\frac{N}{\phi_R}\right)^{1/3} \quad (6)$$

Equation 6 provides the radius of a virtual cluster formed by N tail subunits having diameter σ_{TT} with the overall volume fraction ϕ_R set to a fixed predetermined value (in the present simulations 0.45). Using a value of σ_{ex}, which is chosen to be large enough to negligibly affect the structure of the assemblage, the parameter r_{wall} can be determined. The external potential given by eq 4 acts from the spherical shell and prevents escape of any particle from the simulation cell.

An additional requirement for simulating the assemblage is to ensure that the tail groups are constrained within the cluster volume. This was performed by maintaining a neighbor list[40] of tail groups around each headgroup and preventing the movement of the tail groups outside the regions occupied by the headgroups. The logical steps involved in this procedure were to consider a small spherical region of radius r_{NN} surrounding each headgroup and record the position of all the tail groups within this region. During an attempted move of the tail particle within this radius, a check was made whether the resulting distance of the tail group from the center of mass of the assemblage was greater than the corresponding distance of the headgroup, in which case, the move was rejected with a specified probability. Likewise, when a head particle move was attempted, a similar check was performed to prevent its movement such that its distance from the center of the assemblage was smaller than that of any other tail particle within r_{NN}. This nearest neighbor exclusion was employed to artificially simulate the hydrophilic and hydrophobic properties of head and tail particles, respectively.

The values for the parameters governing the interaction potentials, eqs 1−6, are shown in Table 1. In the simulations, the amphiphilic chains were considered to be composed of $n = 13$ subunits. In most of the simulations, the tail group diameter was assumed to be 0.35 nm. The diameter of a headgroup was assumed to be twice the diameter of a tail group. As stated earlier, the simulations were performed in a spherical simulation cell with impermeable boundaries. In this spherical cell, the particles (subunits) constituting the amphiphilic molecules were initially placed on 92 rays constructed by an icosahedron-based pixelizing method.[41] A total of 13 particles (12 tail groups and 1 headgroup) were placed on

(38) Lee, J. K.; Barker, J. A.; Abraham, F. F. *J. Chem. Phys.* **1973**, *58*, 3166.
(39) Thomson S. M.; Gubbins, K. E.; Walton, J. P. R. B., Chanty, R. A. R., Rowlinson, J. S. *J. Chem. Phys.* **1984**, *81*, 530.
(40) Fincham, D.; Ralston, B. J. *Comput. Phys. Commun.* **1981**, *23*, 127.
(41) Tegmark, M. *ApJ Lett.* **1996**, *470*, L81−L84.

Table 1. Parameters Governing the Interaction Potentials between Various Subunits of an Amphiphilic Chain and the External Potential

type	ϵ/k_BT	σ (nm)	z
TT	2	0.35	−
TH	3	0.525	−
HH	2	0.7	1[a]
Ex	2	1.0×10^2	−

[a] For the electrostatic interaction between the headgroups, the dielectric permeability of the solvent was chosen to be that of water (78.54). The abbreviations TT, TH, HH, and Ex represent tail−tail, tail−head, head−head, and external, resepectively. The simulations were performed at a temperature of 298 K.

each ray of the icosahedron-based structure, with the headgroups located outermost. In other words, the simulations followed the aggregation behavior of 92 amphiphilic chains, each containing 13 subunits (total 1196 particles). The lengths of the rays were governed by the size and number of the tail and headgroups of the amphiphile. The initial placement of the particles in the above manner enhanced the speed of attainment of the equilibrium configuration. All of the simulations were performed at 298 K.

The above model allows the simulation of a molecular assembly without using a lattice approach. Furthermore, the model interaction potentials indirectly incorporate the solvent interactions, thereby eliminating the explicit consideration of the solvent molecules in the simulation. Although the model potentials do not distinguish between the interchain and intrachain interactions between the tail groups, they constitute a better representation of the molecular interactions between various subunits compared to the model potentials used in many lattice-based simulations which completely ignore such bond restrictions.[22] Neglecting the intrachain bonds in the present model avoids the consideration of the reptation movement of the chains,[25] which would invariably render the computations to be more rigorous.

A further point worth noting is that the individual subunits can be of different sizes and merely represent the smallest groups of atoms that can be considered rigid. In this sense, we are essentially freezing some of the bonds in the chains completely (at a level smaller than the subunit size) and compensating for such rigid bonds by neglecting bonds between the subunits comprising a chain. Furthermore, when equilibrating the system in the absence of any shear force, these subunits will fall into the primary minimum, and at equilibrium, any two adjacent tail groups will tend to reside at the van der Waals radius. The neglect of the bonds between the various subunits in a single chain will possibly render the primary equilibrium structure more compact compared to the scenario when the bonds are actually present. On the other hand, the intensity of the shear field (which increases linearly from the center of the assemblage) will be more intense on the peripheral subunits when the bonds are considered as opposed to when the bonds are neglected. These two effects will counterbalance each other, and it is expected that the final (secondary) equilibrium structure of the assemblage in the presence of shear will not be significantly different in the absence or presence of the intrachain bonds.

3. Generation of the Equilibrium Configuration

The computer simulation of the deformation of an assemblage comprises two stages, namely, generation of an equilibrium configuration of the assemblage in the absence of any external shear field and simulation of the deformation of this equilibrium assemblage under the influence of the externally imposed unidirectional shear. The initial equilibrium configuration was obtained using the standard Metropolis Monte Carlo (MMC) technique. Following is a brief description of the procedure adopted in the present study to generate this equilibrium configuration.

3.1. Equilibrium Simulation. The equilibrium simulations were performed using the MMC algorithm.[28,31] As described in the preceding section, the initial configuration of the particles was a regular icosahedron-based structure in a spherical simulation cell with impermeable boundaries. The simulations were performed with a 1:12 number ratio of head to tail groups in the simulation cell. The combination of this number ratio and the employed size ratio of 2:1 between the head and tail groups ensures that the shape of the equilibrium cluster would be spherical. The initial configuration was modified by randomly moving each subunit and determining the energy change associated with the move. The new move is accepted or rejected according to the probability[25,31]

$$p = \begin{cases} 1 & \text{if } (E_{new} - E_{old})/k_BT \le 0 \\ e^{-(E_{new} - E_{old})/k_BT} & \text{otherwise} \end{cases} \quad (7)$$

where E_{new} and E_{old} are the energies of the assemblage in the new and old configurations, respectively, and k_BT is the thermal energy corresponding to the temperature $T = 298$ K. The particles were allowed to equilibrate during about 10^6 simulation steps, following which, the equilibrium property calculations were performed over the next 5×10^4 steps. The total energy of the system was continuously monitored to ensure the attainment of equilibrium. During the simulation, the property calculations were performed after every 10 MC steps and the properties were averaged over 5×10^3 steps. The spatial distribution of head and tail subunits and the aspect ratio of the assemblage were determined from the simulations. The spherical shell was divided radially into 150 segments and the single particle densities (volume fraction) of the head and tail groups were evaluated in each segment.

3.2. Equilibrium Structure of the Assemblage. The equilibrium configuration of the assemblage was monitored after every 10 steps by calculating the total energy of the system and by evaluating the aspect ratio of the assemblage (a detailed discussion on the aspect ratio follows in Section 4). In Figure 1, two simulation snapshots are shown depicting (a) the initial and (b) an equilibrium configuration of the particles. The initial configuration shows the placement of the head and tail subunits on the rays made by the pixelizing method, with the headgroups (light spheres) located at the periphery. The size of the equilibrium cluster (Figure 1b) is observed to be smaller than that of the initial configuration, indicating the coiling (folding) of the amphiphilic chains. The simple potentials used here do not consider specific bond constraints between the tail and headgroups. Despite this, the present model qualitatively emulates the formation of spherical assemblages at equilibrium. The equilibrium radius of the assemblage conforms to that predicted by eq 6 quite closely. Typically, the radius of the assemblage attains a value of about 8−10 times σ_{TT} in the present simulations. This was observed by varying σ_{TT} over 1 order of magnitude. The equilibrium behavior of the assemblage was thus found to be independent of the size of the subunits chosen when the total number of subunits (n) is fixed ($n = 13$ in the present case). This is apparent from the types of interaction potentials used in this study. Both the Lennard−Jones and Coulomb potentials can be expressed as

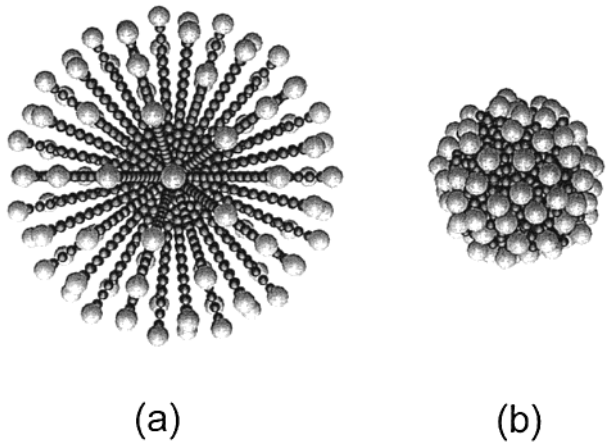

Figure 1. Snapshots of (a) the initial configuration of the assemblage on the rays of an icosahedron with the headgroups (light spheres) of the amphiphilic chains located at the periphery, and (b) an equilibrium configuration of the assemblage. The equilibrium MC simulations were performed using the model of the amphiphilic system described in Section 2 and the parameters given in Table 1.

functions of the scaled separation distance (r/σ), and hence, are scalable for different particle sizes provided the other parameters in the interaction potentials remain fixed. The equilibrium snapshot (Figure 1b) also depicts that the headgroups are located at the periphery of the assemblage with a uniform distribution over the entire surface of the spherical assemblage. Thus, it was confirmed that the combination of the spherical boundary condition and the nearest neighbor exclusion incorporated in the simulations leads to the appropriate partitioning of the head and tail subunits in the periphery and the core of the assemblage, respectively.

The probabilities of occurrence of the head and the tail groups were evaluated at different radial distances from the center of the simulation cell. The typical probability distributions are depicted in Figure 2 as variations of the volume fractions (ϕ) of these groups with the scaled radial distance (r/σ_{TT}). The figure depicts the radial distribution of the tail (dashed line) and head (solid line) subunits averaged over 5000 simulation steps after equilibration. It is apparent that the equilibrium cluster of the particles has a spherical shape with the hydrophilic headgroups located at the periphery. The equilibrium radius of the cluster R_{eq} was obtained as the average distance of the headgroups from the center of the cluster. Thus, R_{eq} can be directly obtained from Figure 2 by evaluating the distance of the peak for the head particles from the origin ($r/\sigma_{TT} = 0$).

4. Simulation of the Shear-Induced Deformation of a Spherical Assemblage

The evolution of the structure of a spherical assemblage generated in the previous section under the influence of external hydrodynamic shear is studied using a modified MC simulation technique that incorporates the hydrodynamic force as a systematic external force biasing the moves of the assemblage subunits. In this section, we present the simulation technique followed by the observations of the structural deformation of the assemblage for various magnitudes of the shear rate.

4.1. Dynamic Simulation. The dynamic simulations were performed using a modified version of the MMC technique, which incorporates a unidirectional linear shear field as an externally imposed systematic hydrodynamic force. The methodology is quite similar to the

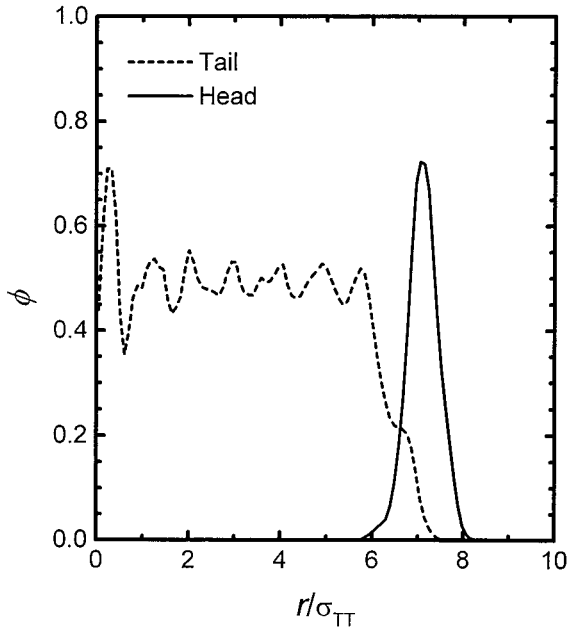

Figure 2. Radial variation of the volume fraction (ϕ) of the tail (dashed line) and head (solid line) groups in a spherical assemblage obtained after equilibration. The lines obtained were averaged over 5000 MC steps after attainment of equilibrium. The axial coordinate is scaled with the tail group diameter. The results were obtained using the potentials described in Section 2 and Table 1.

Force Bias MC or "Smart" MC simulations,[31,42−44] the primary difference being the use of the shear field as the biasing force in the present approach. The additional hydrodynamic force is incorporated in the simulations as an imposed external field that biases the moves of the head and tail groups according to its magnitude and direction. Figure 3 depicts the scheme of the dynamic simulations. A linearly varying shear field from the center of the simulation cell is applied. Assuming that the shear force acts on each particle only along the x direction, the external force on each particle in the spherical shell can be expressed as[45]

$$F_{x,j}(y) = 3\pi\mu\sigma_{jj}\gamma y_j \qquad (8)$$

where σ_{jj} is the diameter of the tail or headgroup, μ is the viscosity, γ is the uniform shear rate, and y_j is the distance of particle j from the center of the cluster along the y direction. The linear shear field implies that the particles lying on the plane of zero shear (the horizontal dashed line) do not experience any shear-induced force, while the particles farthest away from this plane experience the maximum shear force. Moves of all the particles above and below the plane of zero shear will be biased toward the right and left, respectively (Figure 3). After a large number of moves, the final configuration of the particles will represent a distorted cluster. The distortion of the cluster may be followed mathematically by determining the aspect ratio (ratio of the major to the minor radii) of the deformed spheroidal cluster after every few MC steps (each MC step involves successful or attempted moves of all the particles in the cluster).

(42) Pangali, C.; Rao, M.; Berne, B. J. *Chem. Phys. Lett.* **1978**, *55*, 413.
(43) Rao, M.; Berne, B. J. *J. Chem. Phys.* **1979**, *71*, 129.
(44) Rossky, P. J.; Doll, J. D.; Friedman, H. L. *J. Chem. Phys.* **1978**, *69*, 4628.
(45) Dhont, J. K. G. *An Introduction to Dynamics of Colloids*; Elsevier: Amsterdam, 1996.

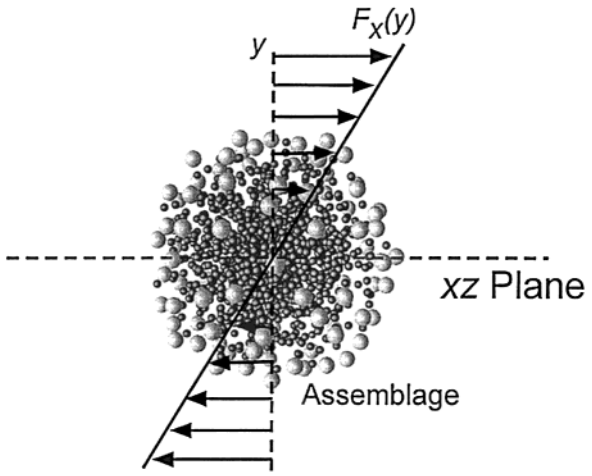

Figure 3. A schematic representation of the dynamic MC simulation procedure in the presence of an external hydrodynamic shear. The variation of the hydrodynamic force F_x (acting along the x direction) with the position along the y direction is given by eq 8. The shear force acts around the origin of the simulation cell. The shear force is largest on the particles at the periphery of the assemblage (the headgroups). The horizontal dashed line represents the plane of zero shear, indicating that any particle whose center lies on this plane does not experience the shear force. The dynamic MC simulations incorporate the hydrodynamic shear as an external force that biases the random moves of the subunit particles in the assemblage along its direction.

The computational procedure employed in the dynamic simulations involves a single particle movement (subunit j in the assemblage) from the old coordinate $\mathbf{R}_j$ to the new coordinate $\mathbf{R}'_j$. Here $\mathbf{R}'_j$ is randomly selected in a domain between $\mathbf{R}'_j - \Delta\mathbf{R}_\theta/2$ and $\mathbf{R}'_j + \Delta\mathbf{R}_\theta/2$ where $\Delta\mathbf{R}_\theta = (\Delta x_0, \Delta y_0, \Delta z_0)$. For simplicity, Δx_0, Δy_0, and Δz_0 are considered to be equal and denoted by Δ. The attempted move is either accepted or rejected according to the probability[31,42,44]

$$p_{FB} = \min\{1, \exp[-\beta(\delta E^{R,R'} + \lambda[\mathbf{F}(\mathbf{R}'_j) + \mathbf{F}(\mathbf{R}_j)]\cdot\delta\mathbf{R}_j + \delta W_{FB})]\} \quad (9)$$

where

$$\delta W_{FB} \cong \frac{\lambda^2\beta\Delta^2}{6}[2\mathbf{F}(\mathbf{R}_j)\cdot\Delta\mathbf{F}(\mathbf{R}_j) + \Delta\mathbf{F}(\mathbf{R}_j)^2] \quad (10)$$

and

$$\Delta\mathbf{F}(\mathbf{R}_j) = \mathbf{F}(\mathbf{R}'_j) - \mathbf{F}(\mathbf{R}_j) \quad (11)$$

In the above equations, $\delta E^{R,R'}$ is the energy change associated with the move, $\mathbf{F}_j$ is the external (along x) force acting on a subunit j in the assemblage, $\delta\mathbf{R}_j$ denotes $\mathbf{R}'_j - \mathbf{R}_j$ in the domain, and $\beta = 1/k_BT$. The hydrodynamic force given by eq 8 was used in eq 9 in the present calculations. The parameter λ dictates the importance of the force bias in the simulation, with $\lambda = 0$ yielding the MMC limit (no external force bias). In the present study, the parameter was fixed at 0.5 for the dynamic simulations, while the step-size Δ was continuously adjusted to yield an acceptance ratio of ca. 50%.[46] It should be noted that we have biased the moves in these dynamic simulations selectively on the basis of the shear force which is a nonconservative (dissipative) force. The rationale behind such an approach is described in greater detail in Appendix A.

(46) Mark, P. D.; Stuart A. R. *Chem. Phys. Lett.* **1981**, *77*, 630.

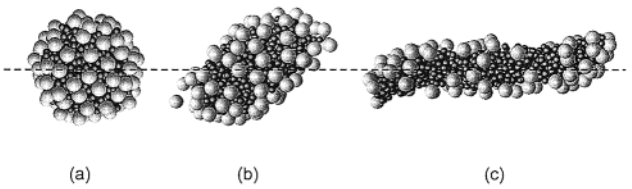

Figure 4. Snapshots of an (a) initial, (b) intermediate, and (c) final configuration of an assemblage under the influence of hydrodynamic shear. The snapshot (b) was taken before attainment of a secondary "dynamic" equilibrium, whereas snapshot (c) represents the shape of the assemblage in the secondary equilibrium. The horizontal dashed line represents the plane of zero shear. The dynamic simulations were performed using the same model as in the equilibrium Monte Carlo simulations. The external hydrodynamic force was assumed to be a linearly varying shear force (see Figure 3). The shear rate γ was 10^{12} s^{-1} in these simulations. This enormous shear was required to deform the assemblage because the length scale of the assemblage was chosen to be extremely small (σ_{TT} = 0.35 nm, giving an equilibrium assemblage radius, $R_{eq} \approx$ 2.36 nm). It is evident that small assemblages will not be affected by the modest shear rates typically encountered in hydrodynamic processes.

The dynamic simulations were performed using the same molecular model as used in generation of the equilibrium configuration. The additional force term in the simulations was determined from eq 8 using shear rates ranging from 10^8 to 10^{12} sec^{-1} and considering the solvent viscosity to be that representing pure water (1×10^{-3} N s m^{-2}). The very high shear rate was necessary to observe any deformation of the assemblage because the length scale of the smallest rigid subunit was extremely small (0.35 nm). A few additional simulations were also performed by varying the size of the smallest subunits (tail groups) keeping the same size ratio of 2:1 between the head and tail groups, in which case, the deformation was observed at much lower shear rates. As in the equilibrium simulations, the dynamic simulations were performed for a large number of steps ($>10^5$) before attainment of the secondary equilibrium, following which the property calculations were performed over the remaining 5×10^4 steps. The total energy of the system was monitored during the simulation to ascertain the attainment of the secondary equilibrium.

4.2. Modifications of Cluster Shape in the Presence of Shear. Figure 4 depicts snapshots from a dynamic simulation showing the evolution of the shape of the cluster under a given shear field. Starting from the equilibrium spherical cluster, Figure 4a (obtained in Section 3), the aggregate becomes increasingly distorted (Figure 4b) and finally attains an elongated spheroidal shape at the secondary equilibrium (Figure 4c). The final configuration in Figure 4c represents an equilibrium configuration of the aggregate under the externally imposed shear field. This secondary equilibrium configuration may be regarded as the shape of the aggregate in the presence of hydrodynamic shear in a dilute suspension. It is evident that under a sufficiently strong shear field relative to the size of the assemblage, the assemblage attains a nearly spheroidal shape with its major axis biased toward the direction of the extensional flow.[45] The presence of shear does not alter the general structural features of the assemblage, because the headgroups still exist at the periphery of the assemblage. It is, however, observed that unlike the initial equilibrium structure shown in Figure 1b, the headgroups in Figure 4c are unevenly distributed

at the surface of the deformed aggregate, tending to congregate toward the ends of the spheroidal assemblage. This feature may result from not explicitly considering a fixed chemical bond between the head and the tail groups in an amphiphilic chain. However, it suggests that in a shear field there will be an uneven distribution of the headgroups on the surface of the assemblage with possibilities of nonuniform charge densities on the deformed aggregate.

The influence of the shear rate on the cluster shape is determined by considering the aspect ratio of the deformed aggregate. The aspect ratio is defined as

$$\textit{aspect ratio} = \frac{\langle R_l \rangle - \langle R_s \rangle}{\langle R_l \rangle + \langle R_s \rangle} \tag{12}$$

where R_l and R_s represent the semimajor and semiminor axes of the spheroidal aggregate, respectively. The terms R_l and R_s were determined by locating the positions of the farthest and the nearest headgroups from the center of the simulation cell, respectively. In the notation of eq 12, the aspect ratio should ideally be zero for a spherical particle, and should attain a value of 1 for a cylindrical particle. The aspect ratio was averaged over about 5×10^3 steps after attainment of the secondary equilibrium.

The combined influence of the shear rate, the interactions between the molecular subunits of the assemblage, and the sizes of these subunits can be represented in terms of the Peclet number

$$\mathrm{Pe} = \frac{3\pi\mu\sigma_{TT}^2\gamma R_{eq}}{k_B T} \tag{13}$$

where R_{eq} is the equilibrium radius of the spherical aggregate, k_B is the Boltzmann constant, and T is the absolute temperature. The Peclet number may be defined here as the ratio of the hydrodynamic (shear) force to the intermolecular (cohesive) force that holds the assemblage together. The incorporation of two different length scales, namely, the tail group diameter σ_{TT} and the equilibrium radius of the assemblage R_{eq} in the Peclet number, provides an indirect way of estimating the strength of the cohesive force that holds the assemblage together and the rigidity of the assemblage. Whereas the tail group radius provides the size of the smallest rigid subunit, the parameter R_{eq} determines the overall size of the assemblage. Note that R_{eq} primarily depends on the Lennard−Jones parameters between the tail groups owing to the abundance of these groups in an assemblage. For a fixed number of subunits in an amphiphilic chain, R_{eq} increases as the magnitude of the attractive interaction potential decreases. In such cases, the Peclet number will become larger, indicating a dominance of the shear forces over the intermolecular (cohesive) forces. Thus, the ratio R_{eq}/σ_{TT} can provide a considerable insight into the structural rigidity of an assemblage. Note also that the potentials used in this study render the interaction energies and forces scalable for different particle sizes. Consequently, the Peclet number alone can provide a comprehensive insight into the shear-induced deformation of the assemblages of different sizes.

A plot of the aspect ratio against the Peclet number provides a quantitative estimate of the extent of deformation due to hydrodynamic shear. Figure 5 shows the variation of the aspect ratio with Peclet number. To obtain the variation of the aspect ratio with the Peclet number, two types of simulations were performed. First, the Peclet number was varied by varying the shear rate for a fixed value of σ_{TT} (solid symbols). Second, the Peclet number was obtained for a fixed shear rate by varying σ_{TT} and keeping the head to tail group size ratio fixed at 2:1 (open symbols). It is evident that below Pe = 1, the hydrodynamic shear cannot modify the equilibrium structure of the aggregate. However, when Pe > 1, the aggregate shape is modified from the equilibrium configuration. As the Peclet number reaches zero, the aspect ratio attains a value of ca. 0.123. The aspect ratio does not ideally vanish as Pe → 0 because even in the absence of hydrodynamic forces (equilibrium), the positions of the headgroups fluctuate, and do not necessarily lead to a perfectly spherical shape of the assemblage. The aspect ratio increases almost linearly with logarithm of the Peclet number. The scaling nature of the interaction potentials for different sizes of the subunits is also apparent from Figure 5 because the simulation results obtained by varying the shear rate and the tail group diameter (closed and open symbols, respectively) are nearly identical.

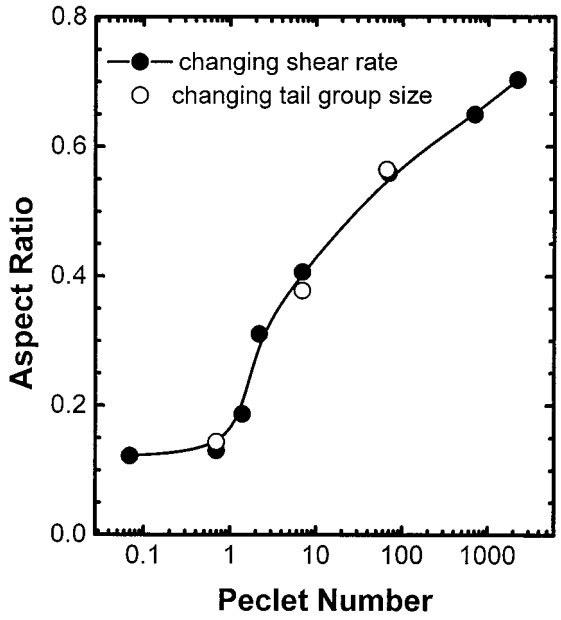

Figure 5. Variation of the aspect ratio of a deformable assemblage with the Peclet number showing the relative influence of the shear rate, assemblage size, and the cohesive forces between the subunits of the assemblage on the extent of shear-induced deformation. Two types of simulations were performed to obtain the results. The Peclet number (see eq 13) was varied by changing the shear rate and keeping the tail group diameter fixed to obtain the solid symbols. In the second type of simulation, the Peclet number was varied by changing the tail group diameter while using a fixed value of γ (open symbols). The similarity of the two results suggests that for the statistical mechanical model used in these simulations, the interaction energy can be scaled with particle size. This helps in identifying the Peclet number as a unique dimensionless group for studying the relative influence of hydrodynamic shear and particle size on the extent of shear-induced deformation of assemblages.

On the basis of these results, it may be deduced that the shear-induced deformation in laminar flow regimes is discernible only for aggregates larger than ca. 100 nm. For smaller aggregates, intense turbulence is required to modify the shapes of the clusters. However, because sizes of these aggregates are strongly dependent on the chemical conditions (such as ionic strength),[2] the influence of hydrodynamic shear on deformation of such aggregates is closely coupled with the chemical environment of the aggregates. Nevertheless, it may be safely concluded from these simulations that micelles or vesicles (with radii

generally less than 10 nm) should retain their equilibrium shapes in the presence of hydrodynamic shear fields typically attained in most dynamic processes. Large assemblages, for instance microemulsions or emulsion droplets, may, however, be deformed under these circumstances.

Finally, from eq 13 it can be observed that the influence of hydrodynamic shear on the aggregate shape is coupled with the aggregate size as well as the sizes of the individual subunits constituting the aggregate. This indicates that variation of the parameter n (number of subunits in an amphiphilic chain) can lead to a different behavior of the aspect ratio with variations in the Peclet number. We note that a smaller value of n together with a larger σ_{TT} would imply a more rigid amphiphilic chain. Consequently, the deformation under shear is expected to be less prominent for such cases.

5. Discussion

The simulation procedures delineated above employ a molecular model of interparticle interactions, which is considerably simpler than more detailed computer simulations employing rigorous models that incorporate the exact molecular architecture of the system. On the other hand, the developed model is considerably more detailed than the continuum level description of interparticle potentials acting between the complete supramolecular assemblages. This feature enables a study of the structural modifications in a macromolecular system arising from deformation of the assemblages. Noting that computer simulation of a system of particles should almost universally assume the rigidity of a particle at some level, it is extremely difficult to employ continuum level potentials in such simulations because this requires redefining the potential each time the shape of the assemblage (or particle) undergoes modification. In this context, the present level of simulation provides an effective compromise by considering subunits of the assemblage as rigid entities, which interact through appropriately defined interaction potentials. This simplification allows a continuous modification of the structure of the assemblage during a simulation without modifying the governing interaction potential.

An important feature of the present model is its ability to predict the secondary equilibrium structure of a single assemblage in a hydrodynamic shear field. The simulated profiles shown in Figure 4 are in remarkable qualitative agreement with experimental profiles of droplets in a unidirectional shear field.[15,16] This indicates that if a suitable means of evaluating the potentials between various constituent groups of a deformable assemblage at equilibrium can be formulated, then the structural changes of such assemblages may be determined using computer simulations based on the present model.

In many flow processes involving polyelectrolyte clusters and emulsions, the presence of shear may alter the shapes of the clusters depending on their size. Computer simulations of the above type can provide insight to the extent of shear induced deformation of such clusters, and help in identifying the limiting shear rates to be employed in such processes to avoid deformation. An additional concern in the presence of shear-induced deformation involves adsorption or solubilization of various species in these clusters, where the capacity of adsorption is directly proportional to the available surface area of these clusters. It is implied from the simulations that the deformation of a droplet can increase the specific surface area of the droplets and, consequently, the number of available sites for adsorption.

It is evident from the simulation results that the structural deformation of the assemblages with $R_{eq} < 100$ nm should not occur under laminar shear rates. This implies that in processes involving micellar systems, the micelles may be treated as rigid particles. However, for larger assemblages, shear will play a significant role in the deformation of the particle shape, and consequently on many equilibrium and dynamic properties of the system.

Several simplifying assumptions were made regarding the system during the simulations. First, the initial (equilibrium) configuration was presumed to be spherical by specifically assigning the head to tail group size ratio as 2:1 and using a head to tail group number ratio as 1:12. This assumption can be relaxed considerably when developing the model, and assemblages of other shapes can easily be generated. It may be noted that the equilibrium structure can perhaps be determined experimentally, and availability of such a technique can facilitate the determination of various parameters governing the interactions between the constituent groups. Second, the shear rate was assumed to be linear, which is quite restrictive in the sense that we assume a viscosity ratio of 1 for the fluids in the internal and external phases. Changing the behavior of the shear can generate different shapes of the aggregate. Indeed, continuum level studies based on solution of Navier−Stokes equations for multiphase flows suggest that as the viscosity ratio increases, the assemblages (or droplets) will tend to be more rigid.[47] Indeed, one of the limitations of the present simulations arises from the drastic simplification concerning the hydrodynamic interactions between the subunits. Here, we have not considered any close range hydrodynamic forces between the subunits, although we might include these in the definition of the parameter A (which is related to the diffusion tensor) in eq A.7 (Appendix A). Finally, in the dynamic simulations, we assumed a single isolated cluster in a shear field. In actual systems, the presence of neighboring assemblages should also affect the structural modifications. In this respect, the present simulation results should be interpreted as as those observed in the limit of zero particle (assemblage) concentration. The interactions between the headgroups and the shear forces must be defined appropriately when considering a periodic system by incorporating suitable long-range corrections.

6. Concluding Remarks

Computer simulations using approximate molecular models for the interaction between various species can be used to emulate the aggregation of deformable clusters. These simulations, on one hand, are more general than lattice based simulations or simple thermodynamic descriptions, while on the other hand, are remarkably simpler than detailed simulations based on ab initio potentials. Influence of hydrodynamic shear on deformable aggregates can be simulated on the basis of such simplified models using the modified dynamic simulation technique which superimposes the systematic hydrodynamic force to bias the moves of the subunits in the traditional MMC method. Representative simulations presented in this study indicate that the laminar shear rates can result in discernible modifications of the aggregate shapes only when such aggregates are larger than ca. 100 nm. For smaller particles, hydrodynamic shear does not alter the equilibrium structure. The findings of these simulation studies may be useful in quantification of the influence

(47) Loewenberg, M.; Hinch, E. J. *J. Fluid Mech.* **1997**, *338*, 299.

of hydrodynamic shear on deformable particles under several practical situations involving flow of emulsion droplets or solubilization of ions or organics in deformable clusters.

Acknowledgment. The authors acknowledge the support of the National Science Foundation under Research Grant BES-9996240 (formerly BES-9705717) and the UCLA Center for Environmental Risk Reduction.

Appendix A

In this appendix we briefly describe the rationale behind using the nonconservative shear force term to bias the moves using the acceptance probability given by eq 9. For this purpose, we first resort to the arguments used in the mesoscopic simulation methods such as Brownian dynamics[31,48] or dissipative particle dynamics,[49−51] and relate these to the underlying mechanisms of moving the particles through the phase space in smart MC techniques.

The typical discrete time step evolution equation for particle positions in an N particle system can be represented as[29,31]

$$\delta\mathbf{r}_i = \beta \sum_{i=1,j=i}^{N} \mathbf{D}_{ij}\cdot\mathbf{F}_j\delta t + \nabla\cdot\mathbf{D}_{ij}\delta t + \delta\mathbf{r}_i^{\mathrm{G}} \qquad \text{(A.1)}$$

where $\mathbf{D}_{ij}$ is the diffusion tensor (in this case represented by the Oseen tensor, which renders the term $\nabla\cdot\mathbf{D}_{ij} = 0$ [29], $\beta = 1/k_{\mathrm{B}}T$, $\mathbf{F}_j$ is the total force acting on a particle, δt is the time step, and the components of the random displacement vector $\delta\mathbf{r}_i^{\mathrm{G}}$ are selected from a Gaussian distribution with zero mean and a covariance matrix given by

$$\langle\delta\mathbf{r}_i^{\mathrm{G}}\delta\mathbf{r}_j^{\mathrm{G}}\rangle = 2\mathbf{D}_{ij}\delta t \qquad \text{(A.2)}$$

The above formalism is the basis of the Brownian dynamics simulations. It should be noted that the force $\mathbf{F}_j$ in eq A.1 can be a combination of conservative and dissipative terms.[49] Shear forces can be incorporated in such simulations as an additional nonconservative (dissipative) force.[49,50] When dissipative forces are incorporated in eq A.1, it becomes analogous to the evolution equations used in dissipative particle dynamics (DPD) simulations.[49]

Smart MC techniques[44] are based on eq A.1, which is used to describe the trial displacement of an individual particle from state m to state n. This trial move may be represented as[31,44]

$$\delta\mathbf{r}_i^{nm} = \beta A\mathbf{F}_i + \delta\mathbf{r}_i^{\mathrm{G}} \qquad \text{(A.3)}$$

where $A = D_{ij}\delta t$ is treated as an adjustable parameter governing the move. We may still assume that the force term in eq A.3 is a sum of conservative and dissipative forces. The acceptance ratio for this type of a move is given by

$$p = \min\left\{1,\exp\left[-\beta\left(\delta E_{\mathrm{nm}} + \frac{1}{2}(\mathbf{F}_i^{n} + \mathbf{F}_i^{m})\cdot\delta\mathbf{r}_i^{nm} + \delta W\right)\right]\right\} \qquad \text{(A.4)}$$

where (see eq 10),

$$\delta W = \frac{\beta A}{4}[(\delta\mathbf{F}_i^{nm})^2 + 2\mathbf{F}_i^{m}\cdot\delta\mathbf{F}_i^{nm}] \qquad \text{(A.5)}$$

and δE_{nm} is the energy difference between the states n and m. Consideration of the conservative and dissipative forces explicitly in the above expression yields

$$\begin{aligned}\delta W &= \delta W^{\mathrm{C}} + \delta W^{\mathrm{D}} + \delta W^{\mathrm{I}}\\ &= \frac{\beta A}{4}[(\delta\mathbf{F}_i^{Cnm})^2 + 2\mathbf{F}_i^{Cm}\cdot\delta\mathbf{F}_i^{Cnm}]\\ &+ \frac{\beta A}{4}[(\delta\mathbf{F}_i^{Dnm})^2 + 2\mathbf{F}_i^{Dm}\cdot\delta\mathbf{F}_i^{Dnm}]\\ &+ \frac{\beta A}{2}[\delta\mathbf{F}_i^{Cnm}\cdot\delta\mathbf{F}_i^{Dnm} + \mathbf{F}_i^{Cm}\cdot\delta\mathbf{F}_i^{Dnm} + \mathbf{F}_i^{Dm}\cdot\delta\mathbf{F}_i^{Cnm}]\end{aligned} \qquad \text{(A.6)}$$

where the superscripts C, D, and I represent conservative, dissipative, and interaction terms, respectively. The interaction term arises from cross-coupling of the conservative and dissipative forces. This is the generalized transition probability that should ideally be used in the force-biased MC method in the presence of dissipative forces. In the present study, we have biased the moves only on the basis of the dissipative forces, suggesting that the associated conservative system evolves only on the basis of the Metropolis algorithm. In other words, the potential governing the conservative forces is already considered in the acceptance ratio. Thus, we have considered an acceptance ratio of the general form

$$p = \min\left\{1,\exp\left[-\beta\left(\begin{array}{c}\delta E_{nm} + \omega_C\left(\frac{1}{2}(\mathbf{F}_i^{Cn} + \mathbf{F}_i^{Cm})\cdot\delta\mathbf{r}_i^{nm} + \delta W^{\mathrm{C}}\right)\\ + \omega_{\mathrm{D}}\left(\frac{1}{2}(\mathbf{F}_i^{Dn} + \mathbf{F}_i^{Dm})\cdot\delta\mathbf{r}_i^{nm} + \delta W^{\mathrm{D}}\right) + \omega_{\mathrm{I}}\delta W^{\mathrm{I}}\end{array}\right)\right]\right\} \qquad \text{(A.7)}$$

where the weighting factors (ω) for the conservative, dissipative, and interaction components are chosen as $\omega_{\mathrm{C}} = \omega_{\mathrm{I}} = 0$ and $\omega_{\mathrm{D}} = 1$. In this sense, our simulations simply bias the directions of the attempted moves toward the shear force, and are not very different from some earlier nonequilibrium MC simulations that studied the influence of an external shear field on deformable entities by incorporating a higher jump rate in the flow direction.[35] The main difference is that we have changed the intensity of the bias as a linear function (γy) of the distance of the subunits from the center of the assemblage. The manners in which various forces and the simulation cell have been defined in this study allow the use of the acceptance ratio described above. It is, however, unclear whether such an approach will be valid in the thermodynamic limit or for a periodic system. Finally, we note that eq A.7 with the weighting factors shown above will become identical to eq 9 when $\lambda = 0.5$ and $A = \Delta^2/6$,[31] as has been used in the simulations.

Note that in the limit of simultaneous N particle moves with small step sizes, the present simulations in the absence of dissipative forces will be almost identical to Brownian dynamics,[31,48] whereas in the presence of the dissipative forces, under certain constraints, they will

(48) Cascales, J. J. L.; DelaTorre, J. G. *J. Chem. Phys.* **1991**, *95*, 9384.
(49) Marsh, C. Theoretical Aspects of Dissipative Particle Dynamics, Doctoral Dissertation, Theoretical Physics, University of Oxford, U.K., 1998.
(50) Clark, A. T.; Lal, M.; Ruddock, J. N.; Warren, P. B. *Langmuir* **2000**, *16*, 6342.
(51) Groot, R. D. *Langmuir* **2000**, *16*, 7493.

resemble dissipative particle dynamics.[49,50] Although it is known that such simulations are inappropriate for short time evolution of the system, it is expected that the long time behaviors of the system are well represented by these simulations.[31,49] Extending this argument, we might state that the present MC simulations will provide a realistic description of the long-time behavior, or the secondary equilibrium structure, the determination of which is the primary objective of the present study.

Appendix B

Nomenclature

A	parameter defined in eq A.3
$\mathbf{D}_{ij}$	diffusion tensor
D_{ij}	diffusion coefficient
e	electronic charge (1.6×10^{-19} C)
E_{new}	total energy of the assemblage in the new configuration
E_{old}	total energy of the assemblage in the old configuration
$\mathbf{F}$	force vector used in the biased Monte Carlo simulation
$F_{x,j}$ (y_j)	external hydrodynamic force along the x direction acting on particle j
k_B	Boltzmann constant (1.38×10^{-23} JK^{-1})
N	number of tail groups in an assemblage
n	number of subunits in an amphiphilic chain
Pe	Peclet number defined in eq 12
p	acceptance probability of a move in Metropolis Monte Carlo technique
p_{FB}	acceptance probability of a move in biased Monte Carlo simulation
$\mathbf{R}_j$	coordinates of particle j
R_{eq}	radius of the equilibrium configuration of the assemblage (in absence of shear)
R_l	semimajor axis of the spheroidal assemblage
R_s	semiminor axis of the spheroidal assemblage
$\mathbf{r}_i$	position vector of particle i
r	radial distance
r_{ran}	range of the external interaction potential
r_{wall}	radial distance of the spherical boundary from the center of simulation cell
T	temperature (K)
U_{ex}	external potential acting from the boundary
U_{HH}	head−head interaction potential
U_{TH}	tail−head interaction potential
U_{TT}	tail−tail interaction potential
x	coordinate direction in which the shear acts
y_j	distance of particle j from the origin along the y direction
z	charge number on a headgroup

Greek Symbols

β	$1/k_BT$
Δ	stepsize during a biased Monte Carlo move
ϵ_{ex}	Lennard−Jones parameter for the external potential
ϵ_{HH}	Lennard−Jones parameter for the head−head interaction energy
ϵ_{TH}	Lennard−Jones parameter for the tail−head interaction energy
ϵ_{TT}	Lennard−Jones parameter for the tail−tail interaction energy
ϵ_0	dielectric permittivity of vacuum (8.854×10^{-12} C^{2}N^{-1}m^{-2})
ϵ_r	dielectric constant of the solvent (78.54 for water)
$\Delta\boldsymbol{F}$	force change associated with a move
δW_{FB}	normalization constant defined in eq 10
ϕ_R	volume fraction of tail groups
γ	shear rate
λ	parameter used in dynamic simulation, eq 9
μ	solvent viscosity
σ_{ex}	hypothetical distance used in defining the external potential, eqs 4 and 5
σ_{HH}	headgroup diameter
σ_{TH}	$(\sigma_{HH} + \sigma_{TT})/2$
σ_{TT}	tail group diameter
ω	weighting parameter defined in eq A.7

LA001108V